ResearchGate

See discussions, stats, and author profiles for this publication at: https://www.researchgate.net/publication/12263817

Numerical simulation of cavitation bubble dynamics induced by ultrasound wave

ARTICLE *in* ULTRASONICS SONOCHEMISTRY · NOVEMBER 2000

Impact Factor: 4.32 · DOI: 10.1016/S1350-4177(00)00059-6 · Source: PubMed

CITATIONS
41

READS
159

5 AUTHORS, INCLUDING:

Alain Gerard
University of Bordeaux
147 PUBLICATIONS **648** CITATIONS
SEE PROFILE

Alejandro Hita
Austral University (Argentina)
28 PUBLICATIONS **169** CITATIONS
SEE PROFILE

Available from: Alejandro Hita
Retrieved on: 26 January 2016

ELSEVIER

Ultrasonics Sonochemistry 7 (2000) 217–227

Ultrasonics SONOCHEMISTRY

www.elsevier.nl/locate/ultsonch

Numerical simulation of cavitation bubble dynamics induced by ultrasound waves in a high frequency reactor

G. Servant [a,c,*], J.P. Caltagirone [a], A. Gérard [b], J.L. Laborde [c], A. Hita [c]

[a] *Laboratoire de Modélisation Avancée des Systèmes Thermiques et Écoulements Réels (ENSCPB), Avenue Pey-Berland, B.P. 108, 33402 Talence Cedex, France*

[b] *Laboratoire de Mécanique Physique, Université Bordeaux I, 351 cours de la Libération, 33405 Talence Cedex, France*

[c] *EDF-Div. R&D/Application de l'Électricité dans l'Industrie, Route de Sens-Ecuelles, 77818 Moret-sur-Loing Cedex, France*

Abstract

The use of high frequency ultrasound in chemical systems is of major interest to optimize chemical procedures. Characterization of an open air 477 kHz ultrasound reactor shows that, because of the collapse of transient cavitation bubbles and pulsation of stable cavitation bubbles, chemical reactions are enhanced. Numerical modelling is undertaken to determine the spatio-temporal evolution of cavitation bubbles. The calculus of the emergence of cavitation bubbles due to the acoustic driving (by taking into account interactions between the sound field and bubbles' distribution) gives a cartography of bubbles' emergence within the reactor. Computation of their motion induced by the pressure gradients occurring in the reactor show that they migrate to the pressure nodes. Computed bubbles levitation sites gives a cartography of the chemical activity of ultrasound. Modelling of stable cavitation bubbles' motion induced by the motion of the liquid gives some insight on degassing phenomena. © 2000 Elsevier Science B.V. All rights reserved.

Keywords: Caflisch equations; Cavitation bubbles; Degassing effect; Sonochemical reactor; Sonochemistry; Transient bubble motion; Wave attenuation

1. Introduction

Power ultrasound has significant effects on rates of various processes in chemical processes. In a high frequency reactor, ultrasounds have the property of enhancing chemical reactions, such has breaking H_2O molecules which leads to radical (OH^0) production. Much practical and theoretical work has been done aimed at a better understanding of the phenomena occurring. Even so, acoustic cavitation is not a such a well-known phenomenon. Indeed, acoustic cavitation causes a wide range of phenomena. Because of the emergence of cavitation bubbles, the acoustic behaviour of the liquid is profoundly affected. For instance, there is strong absorption of sound and a change occurs in the average density and sound speed of the bubbly liquid [1]. These bubbles collapse in one cycle and fragment into smaller bubbles, called transient bubbles. These bubbles gather in a ball-shaped cloud, and because of the pressure gradients induced by the wave propagation they migrate to pressure nodes [2]. Then transient clouds disappear bumping into spider-like clouds. Their daughter bubbles grow by rectified diffusion and levitate. The latter bubbles are called stable cavitation bubbles. These stable bubbles are responsible for the chemical activity of cavitation [3]. Some of them are torn off the pressure nodes by the fluid convection motion induced by the temperature gradients occurring between the bulk fluid and the transducer that heats it. When they reach the water–air interface, they evaporate and participate in the degassing of the liquid. Modelling these phenomena, and taking into account the interactions between them, will greatly helps in scaling-up sonoreactors.

In particular, knowing both the sound pressure field distribution in the bubbly liquid and the dynamics of both transient and stable cavitation bubbles (i.e., the bubble velocity field within the reactor) will help us to determine where chemical reactions take place.

In this paper, we propose to model a 'cavitation cycle' in a high frequency open air reactor. By 'cavitation cycle', we mean the spatial-temporal evolution of cavitation bubbles from their birth to their evaporation. We first consider phenomena such as the emergence of

* Corresponding author. Fax: 33-0 160737146.
E-mail address: guillaume.servant@edf.fr (G. Servant)

1350-4177/00/$ - see front matter © 2000 Elsevier Science B.V. All rights reserved.
PII: S1350-4177(00)00059-6

cavitation bubbles due to the acoustic driving. For clarity, we refer to these bubbles as bubbles 'A'. Coupling between the sound field and the bubble distribution is taken in account.

We then consider the migration of cavitation bubbles induced by the wave propagation (bubbles 'B'). Finally, we pay attention to the degassing of the fluid. We model the convection flow that tears off some stable cavitation bubbles that participate in the degassing of the fluid (since they evaporate when they reach the water–air interface). These bubbles are referred to as bubbles 'C'.

2. Theory and background

To model the sound field in a bubbly liquid, the majority of past efforts were based on the solution of idealized problems, such as a one-dimensional wavefront propagating in a 'channel'. Most investigation dealt with analytical solutions of problems by expanding the wave equation into an infinite series. Recently, numerical solutions have been presented in the literature. In Refs. [4–7] simulations were made in sonochemical reactors of complex geometries using adapted wave propagation equations to take into account damping and phase change due to the presence of bubbles. In Refs. [8,9] the calculus in a one-dimensional geometry was made but using a more complex bubble dynamic equation. Our approach is based on the Caflisch model [10].

2.1. Emergence of cavitation bubbles

Gas bubbles in a liquid affect profoundly the acoustic behaviour of the liquid. Dispersion and attenuation of the ultrasound occurs [11]. For example, the sound velocity in water is $1500\ \mathrm{m\ s^{-1}}$, whereas in a bubbly liquid it may decrease to $20\ \mathrm{m\ s^{-1}}$, which is well below the velocity of sound in air (about $340\ \mathrm{m\ s^{-1}}$).

2.1.1. Dependence of the bubble volume fraction and the pressure amplitude

Although there are some recent publications [1,12], few data are available on bubble volume fraction and radii distribution of cavitation bubbles in sonochemical reactors. Therefore, as a first step, we make the following assumption: because an ultrasound wave propagates within a liquid, generation of bubbles occurs. In the present work we take into account the generation of bubbles due to the acoustic driving. We assume a cavitation threshold of 1×10^5; MPa [13]. Concerning the relation between the bubble volume fraction and the acoustic driving, we assume that above the cavitation threshold the bubble volume fraction is set to 0.5%.

The assumed distribution of bubble radii is that of [11]. The bubble volume fraction is given by:

$$\beta(\boldsymbol{r},t)=\frac{4}{3}\int_0^\infty R^3(\boldsymbol{r},R_0,t)f(\boldsymbol{r},R_0)\,\mathrm{d}R_0, \tag{1}$$

where $R(\boldsymbol{r},R_0,t)$ is the instantaneous bubble radius at time t at position $\boldsymbol{r}$ having an equilibrium radius R_0. $f(\boldsymbol{r},R_0)\,\mathrm{d}R_0$ is the number of bubbles per unit volume with equilibrium radius R_0, where f is a truncated Gaussian:

$$f(R_0)=\begin{cases} C\exp[-(R_0-R_3)^2/\sigma^2], & R_1<R<R_2,\\ =0, \quad \text{otherwise.}\end{cases} \tag{2}$$

We assume a bubble radii ranging from $R_1=1\ \mu\mathrm{m}$ and $R_2=1\ \mathrm{mm}$. The deviation σ is set to 2 mm. C is a parameter chosen to match the fixed gas volume void fraction β; $R_3=(R_1+R_2)/2$.

2.1.2. Dynamics of acoustic waves in bubbly liquid

We use a continuum model for the interaction between the sound field and the bubble distribution, that is to say bubble sizes and inter-bubble distances are small compared with the distance over which the macroscopic quantities of the mixture change. In Ref. [14] equations of wave propagation in bubbly liquids were heuristically derived (from the Euler equations), which were confirmed in ref. [10] using a more rigorous derivation:

$$\frac{\partial\rho_1}{\partial t}+\mathrm{div}(\boldsymbol{q})_1=3\beta\rho_{10}\frac{\partial x}{\partial t}, \tag{3}$$

$$\frac{\partial^2x}{\partial t^2}+\delta_{\mathrm{tot}}\frac{\partial x}{\partial t}+\omega_0^2x=\frac{p-p_0}{\rho_{10}R_0^2}, \tag{4}$$

$$\frac{\partial\boldsymbol{q}_1}{\partial t}+\nabla\cdot(\boldsymbol{q}\boldsymbol{u})_1=-\nabla p, \tag{5}$$

where u_1, ρ_1 and ρ_{10} denote respectively the liquid velocity, density, and density at equilibrium. $\boldsymbol{q}=\rho_1\boldsymbol{u}_1$ is the movement quantity of the liquid. p is the pressure of the bubbly liquid. β and c_0 are the bubble volume fraction within the liquid and the sound velocity in the liquid.

Eq. (4) comes from the linearization of the Keller–Kolodner equation [15], by assuming that the bubble equilibrium size radius R_0 fulfils the condition $R_0\ll c/\omega$, and small amplitudes $p\ll p_0$ of the external sound field. The bubble time-dependent radius obeys the expression $R=R_0[1+x(t)]$ with $x\ll1$. Thermal, viscous and radiation losses define the damping constant δ_{tot} for a bubble of radius R_0 [16]:

$$\delta_{\mathrm{tot}}=\delta_{\mathrm{th}}+\delta_{\mu_1}+\delta_{\mathrm{r}}=\frac{p_0+(2\sigma/R_0)}{\rho\omega R_0^2}\,\mathrm{Im}\,\phi+\frac{4\mu_1}{\rho_{10}R_0^2}+\frac{\omega^2R_0}{c_0}, \tag{6}$$

where ϕ is the (complex) phase shift between the sound field and the bubble motion and ω is the transducer pulsation. We use a computational fluid dynamics (CFD) code, called Aquilon [17], to compute the wave propagation in the bubbly liquid. This code solves the Euler equations (as well as the Navier–Stokes equations):

$$\frac{\partial \rho_1}{\partial t} + \operatorname{div}(\rho \boldsymbol{u})_1 = 0, \tag{7}$$

$$\frac{\partial \boldsymbol{q}_1}{\partial t} + \nabla \cdot (\boldsymbol{q}\boldsymbol{u})_1 = -\nabla p. \tag{8}$$

Detailed algorithms to solve Eqs. (7) and (8) can be found in Ref. [17]. In the following section, we present the modification made to the Aquilon code in order to solve the Caflisch equations.

2.1.3. Details of the program implementation

The main difficulty encountered when solving the Caflisch equations is to solve the temporal coupling between the radial displacement x of the bubble and the external pressure $p-p_0$. To solve this problem, we first rewrite Eqs. (4) and (5) in terms of $\rho-\rho_0$, by using the state law of the liquid that relates pressure and density changes:

$$p_1 - p_0 = \frac{1}{\rho_{10}\chi_T}(\rho_1 - \rho_{10}), \tag{9}$$

where p_0 is the atmospheric pressure and χ_T is the compressibility of water.

$$\frac{\partial^2 x}{\partial t^2} + \delta_{tot}\frac{\partial x}{\partial t} + \omega_0^2 x = \frac{\rho_1 - \rho_{10}}{\rho_{10}^2 \chi_T R_0^2}, \tag{10}$$

$$\frac{\partial \boldsymbol{q}_1}{\partial t} + \nabla \cdot (\boldsymbol{q}\boldsymbol{u}_1) = -\frac{1}{\rho_{10}\chi_T}\nabla \rho_1. \tag{11}$$

For clarity, we do not write spatial discretization in the following expressions. Temporal discretization of Eq. (10) yields:

$$x_i^{(n+1)} = \frac{\dfrac{\rho_1^{(n+1)} - \rho_{10}}{\rho_{10}^2 \chi_T R_0^2} + \delta_{tot}\dfrac{x_i^{(n-1)}}{2\,\Delta t} - \dfrac{x_i^{(n-1)} - 2x_i^{(n)}}{\Delta t^2}}{\omega_{0,i}^2 + \dfrac{1}{\Delta t^2} + \dfrac{\delta_{tot,i}}{2\,\Delta t}}, \tag{12}$$

where $x_i^{(n+1)}$ denotes the radial displacement of a bubble having an equilibrium radius $R_{0,i}$, a resonance frequency $\omega_{0,i}$ and a damping constant $\alpha_{tot,i}$.

Thus

$$x_i^{(n+1)} - x_i^{(n)} = \frac{\dfrac{-\rho_1^{(n+1)} - \rho_1^{(n)}}{\rho_0^2 \chi_T R_i^2} + \delta_{tot,i}\dfrac{x_i^{(n-1)} - x_i^{(n-2)}}{2\,\Delta t} - \dfrac{(x_i^{(n-1)} - x_i^{(n-2)}) - 2(x_i^{(n)} - x_i^{(n-1)})}{\Delta t^2}}{\Omega_i}, \tag{13}$$

with

$$\Omega_i = \omega_{0,i}^2 + \frac{1}{\Delta t^2} + \frac{\delta_{tot,i}}{2\,\Delta t}.$$

Discretization of the continuity equation and Euler equation gives:

$$\frac{\rho_1^{(n+1)} - \rho_1^{(n)}}{\Delta t} + \operatorname{div} \boldsymbol{q}^{(n+1)} = 4\pi \sum_{i=1}^{\infty} R_i^3 \frac{x_i^{(n+1)} - x_i^{(n)}}{\Delta t} f_i\, \Delta R_0, \tag{14}$$

$$\frac{\boldsymbol{q}_1^{(n+1)} - \boldsymbol{q}_1^{(n)}}{\Delta t} + \nabla \cdot (\boldsymbol{q}^{(n+1)}\boldsymbol{u}_1^{(n)}) = -\frac{1}{\rho_{10}\chi_T}\nabla \rho^{(n+1)}. \tag{15}$$

By introduction of the expression $(x^{(n+1)} - x^{(n)})$ (derived from Eq. (13)) into Eq. (14), we derive a new expression of density $\rho^{(n+1)}$ of the bubbly liquid:

$$\begin{aligned}\rho_1^{(n+1)} = \rho_1^{(n)} - \Theta\, \Delta t \operatorname{div} \boldsymbol{q}_{i,k}^{(n+1)} + 4\pi\rho_0\Theta \sum_{i=1}^{\infty} \frac{R_i^3}{\Omega_i} f_i\, \Delta R_0 \\ \times \left[\delta_{tot,i} \frac{x_i^{(n-1)} - x_i^{(n-2)}}{2\,\Delta t} \right. \\ \left. - \frac{(x_i^{(n-1)} - x_i^{(n-2)}) - 2(x_i^{(n)} - x_i^{(n-1)})}{\Delta t^2} \right],\end{aligned} \tag{16}$$

with

$$\Theta = \left(1 + 4\pi \sum_{i=1}^{\infty} \frac{R_i f_i\, \Delta R_0}{\rho_0 \chi_T \Omega_j}\right)^{-1}.$$

The set of Eqs. (16), (12) and (15) allows us to solve the wave propagation in a bubbly liquid.

2.2. Spatio-temporal evolution of bubble clouds

Following their emergence, the cavitation bubbles 'A' collapse in the next cycle. In the following section, we describe the method used to model the motion of their daughter bubbles.

2.3. Governing equations

We consider the medium as a bubbly liquid. The model is based on the Eulerian two-fluid approach. Separate Eulerian conservation equations are formulated for both phases coupled through interfacial transfer terms. Each phase is governed by the Navier–Stokes equations. Interactions between the liquid and bubbles (such as added mass force, drag force …) appear in the equations via coupling terms I_k. I_k is obtained

from the analysis of the balance of forces acting on an isolated particle.

These equations can be derived in conservative, transient form as:

$$\frac{\partial(\alpha\rho)_k}{\partial t} + \nabla(\alpha\rho u)_k = 0, \tag{17}$$

$$\frac{\partial(\alpha\rho u)_k}{\partial t} + \nabla\cdot(\alpha\rho u \otimes u)_k = -\nabla\!\rightarrow p_1 + (\alpha\rho)_k g + \mu_k \nabla^2(\alpha u)_k + I_k, \tag{18}$$

$$\frac{\partial T_1}{\partial t} + u_1 \nabla\!\rightarrow T_1 = \alpha \Delta T_1, \tag{19}$$

where p_1 is the mean pressure of the continuous phase and I_k is the part of the interfacial momentum transfer rate between phases. u, ρ, T and μ are respectively velocity, density, temperature and dynamic viscosity. $k=1$ or 2, where 1 refers to the fluid phase and 2 to the bubble phase, a and α are thermal diffusivity of fluid and volume fraction of the considered phase. g is the gravitational force. The CFD code Estet–Astrid solves these equations [18,19].

2.3.1. Interfacial momentum transfer

If we consider a dilute dispersion of small bubbles in translation with relative motions of low Reynolds number, the resultant force induced by the surrounding fluid flow on each point included in the dispersed phase can be written as:

$$\boldsymbol{f}V = \boldsymbol{F}_{\mathrm{D}} + \boldsymbol{F}_{\mathrm{MA}} + \left(\rho V \frac{\mathrm{d}\boldsymbol{u}_1}{\mathrm{d}t} - \rho_1 \boldsymbol{g} V\right), \tag{20}$$

where V is the volume of a bubble.

The first two terms on the right-hand side of Eq. (20) are due to the disturbance flow set up by the particle and correspond to the drag force and the apparent mass force. The last term is due to the stress applied on the bubble by the undisturbed surrounding fluid flow which would occur if the particle were withdrawn. The local balance of the interfacial momentum transfer induces:

$$I_{2,i} = -I_{1,i} = \alpha_2 f, \tag{21}$$

2.4. Bubble motion due to pressure gradient

Since the acoustic waves are propagating, pressure gradients will occur in the bubbly liquid. Thus bubble motion is initiated [4]. Surprisingly, few data are available in the literature with respect to sizes, velocities and densities of bubbles in cavitation fields. In refs. [2,20] the bubble velocity field in a stationary sound field was derived analytically and compared with experimental data with good agreement. More recently, in Ref. [21] the clustering of the bubbles near pressure antinodes in a standing wave was modelled. Comparison with experiments gave good agreement. In the present work, we focus our attention on the translational motion of transient cavitation bubbles towards pressure nodes.

2.4.1. Forces exerted on the bubbles

We assume that the bubbles considered (transient bubbles 'B') have the same equilibrium radius that follows linear oscillations (cf. Eq. (4)).

Forces experienced by the transient bubbles 'B' are as follows:

- The added mass force,

$$\boldsymbol{F}_{\mathrm{MA}} = \tfrac{1}{2}\rho_1 V(t)\frac{\mathrm{d}\boldsymbol{u}_r}{\mathrm{d}t}. \tag{22}$$

- The expression of the viscous drag force is that derived analytically in Ref. [22] considering a time-dependent radius:

$$\boldsymbol{F}_{\mathrm{D}} = -12piR(t)\mu_1\boldsymbol{u}_r. \tag{23}$$

- The force applied to the bubble by the undisturbed surrounding fluid flow, $\rho_1 V(t)\mathrm{d}u_1/\mathrm{d}t$ (gravity is neglected in this paper).

Here u_r is the local instantaneous relative velocity at each point included in the dispersed phase and given by $u_r = u_2 - u_1$.

To compute the spatio-temporal evolution of cavitation bubbles, due to pressure gradients, we may choose between the following two approaches:

- 'Direct simulation': by direct simulation, we mean calculating simultaneously the wave propagation and the bubbles' migration (by taking into account their time-dependent volume). However, computing the wave propagation needs small time step (below 1 μs). Knowing that time scale of bubble migration is around 1 ms, it is obvious that this approach will be costly in computer time.
- Another way is to compute separately wave propagation and bubbles' migration, assuming that the bubbles do not interact with the sound field. A knowledge of the acoustic pressure field allows us to compute the average force due to the pressure gradient. The advantage of this method is that we do not have to fulfil the restricted time step of the wave propagation computing.

We chose the latter method.

We neglect bubble volume variation, expected in the derivation on the force applied on the bubble by the undisturbed surrounding fluid flow. We consider that bubbles encounter only one sound field amplitude during one of their radial oscillation period (which is assumed equal to the sound field oscillation period $T = 1/f$ for all bubbles). Then the forces are determined as follows, involving time averaging over T:

$$\langle \boldsymbol{F}_{\mathrm{D}} \rangle_T = -12\pi R_0 \mu \boldsymbol{u}_r.$$

$$\langle \boldsymbol{F}_{\mathrm{MA}} \rangle_T = \tfrac{1}{2}\rho_1 V(t)\frac{d\boldsymbol{u}_r}{\boldsymbol{dt}}.$$

- The force applied on the bubble by the undisturbed surrounding fluid flow, $\rho_1 \, du_1/dt$, may have another expression. Referring to the Euler equation, we have $\rho_1 \, du_1/dt, = -\nabla p$, thus $\rho V(t) \, du_1/dt = -V(t)\nabla p$. Hence we retrieve the expression of the primary Bjerknes force $\boldsymbol{F}_{\mathrm{Bj}}$. This force is calculated upon the pressure field computed for the emergence of cavitation bubbles 'A'. This force is introduced in the code as an external force:

$$\langle \boldsymbol{F}_{\mathrm{Bj}} \rangle_T = -\langle V(t) \, \nabla p \rangle_T. \tag{24}$$

We then deduce result force induced by the surrounding fluid flow on each point included in the dispersed:

$$\boldsymbol{fV} = \langle \boldsymbol{F}_{\mathrm{D}} \rangle_T + \langle \boldsymbol{F}_{\mathrm{MA}} \rangle_T + \langle \boldsymbol{F}_{\mathrm{Bj}} \rangle_T. \tag{25}$$

3. Degassing of the liquid

Degassing effects play an important role in the design of sonochemical reactors [23]. In this study, we consider that the transducer that generates ultrasonic waves heats up. Assuming that the transducer heats up, a temperature gradient occurs within the bulk fluid: the transducer temperature remains constant ($\sim 35^{\circ}\mathrm{C}$) and the fluid is initially at a temperature of $20^{\circ}\mathrm{C}$. Thus convection is initiated. A computation has been made considering the fluid as a single phase [3]. The present work takes into account the presence of cavitation bubbles.

We assume that the bubble motion due to the temperature gradient is not influenced by the pressure gradients induced by the wave propagation. This hypothesis comes from the Bjerknes forces analysis. Because we can assume that stable cavitation bubbles have a constant radius through time, the average radiation force, i.e., the Bjerknes force is zero.

We consider stable cavitation bubbles that appear at pressure nodes and those of them that coalesce, having a size greater than the resonance size. For a light particle (with respect to gas density: $\rho_2 \ll \rho_1$) the momentum interfacial transfer term reduces to the drag and added mass force contribution. The drag force contribution can be written as proportional to a coefficient F_{D} given in terms of the particle Reynolds numbers [24]: $-\alpha_2 \rho_1 F_{\mathrm{D}} V_{r,i}$

$$F_{\mathrm{D}} = \frac{3}{4} \frac{C_{\mathrm{D}}}{d} |\boldsymbol{u}_r|. \tag{26}$$

We use the approximate form for the drag force coefficient C_{D} [24]:

$$C_{\mathrm{D}}(\mathrm{Re}) = \frac{24}{\mathrm{Re}} (1 + 0.15\mathrm{Re}^{0.687}), \qquad \text{for } \mathrm{Re} < 1000, \tag{27}$$

with

$$\mathrm{Re} = \frac{\rho_1 |\boldsymbol{u}_r| d_p}{\mu_1}.$$

The added mass force contribution is equal to

$$-\alpha_2 \rho_1 \frac{1}{2} \frac{d\boldsymbol{v}_r}{dt}.$$

The flow of fluid and bubbles is considered as incompressible. The state law of the fluid (water), using the Boussinesq approximation is:

$$\rho_1 = \rho_{10}[1 - \zeta(T - T_0)], \tag{28}$$

where ζ is the expansion coefficient of water and T_0 its initial temperature. The bubble density is assumed to be constant and equal to ρ_{20}.

We model the cavitation bubble (and those which coalesce) by a rigid body, having an average radius of 50 μm (bigger than the resonance size).

4. Modelled reactor

The modelled reactor is 8 cm in diameter and height. The transducer diameter is 3 cm. The geometry is shown in Fig. 1. The transducer frequency is set at 477 kHz, in accordance with the experiments of [3]. The cylindrical sonoreactor has rigid walls. The water surface height is 8 cm.

To gain computing time, all calculations are made on a slice of the reactor of radius 4 cm and with a height of 8 cm.

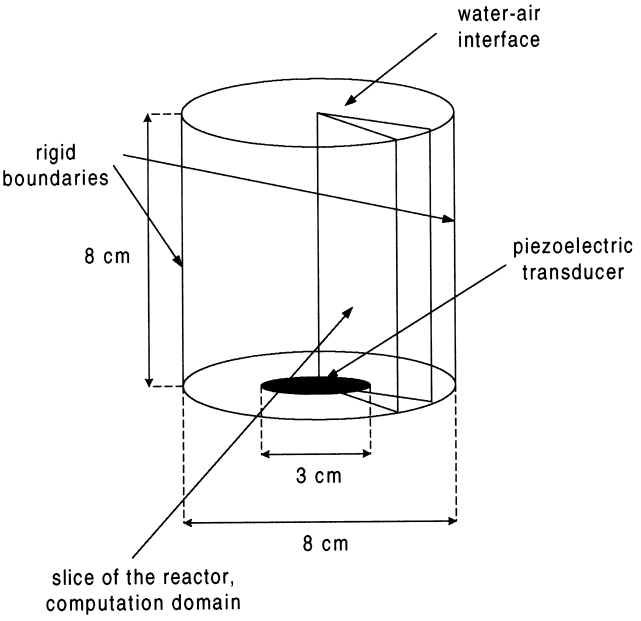

Fig. 1. Modelled sonoreactor and computation domain.

5. Results

5.1. Emergence of cavitation bubbles

5.1.1. Transducer boundary conditions

As the transducer boundary condition it is assumed that the transducer time-dependent velocity $u_0(t)$ is:

$$u_0(t) = \omega A_0 \sin(\omega t), \tag{29}$$

where A_0 is the maximum transducer face displacement and ω is the circular frequency. A_0 is set to 4×10^{-8} m. Fig. 2(b) and (c) illustrate respectively the pressure field in the bubbly liquid and the bubble volume fraction that represents the number of bubbles per unit volume that emerged as a result of the acoustic driving. Comparing these two graphs, as expected, bubbles emerge in the wave propagation zone (reactor diameter less than or equal to 1.5 cm).

Fig. 2(a) shows the pressure field in a liquid without bubbles. Comparing this field with that of the bubbly liquid, differences are slight. However, we notice a darker zone in the vicinity of the water surface, which shows a damping of the wave. To explain this result, we should refer to the calculation of the wave velocity and the attenuation coefficient in the mixture of liquid and bubbles, in the case of a one-dimensional wave front [11]. With the assumed gaussian distribution of bubble radii and a bubble volume fraction of 0.5%, the sound velocity is that of a pure liquid, and the damping is light: 4 dB m^{-1}.

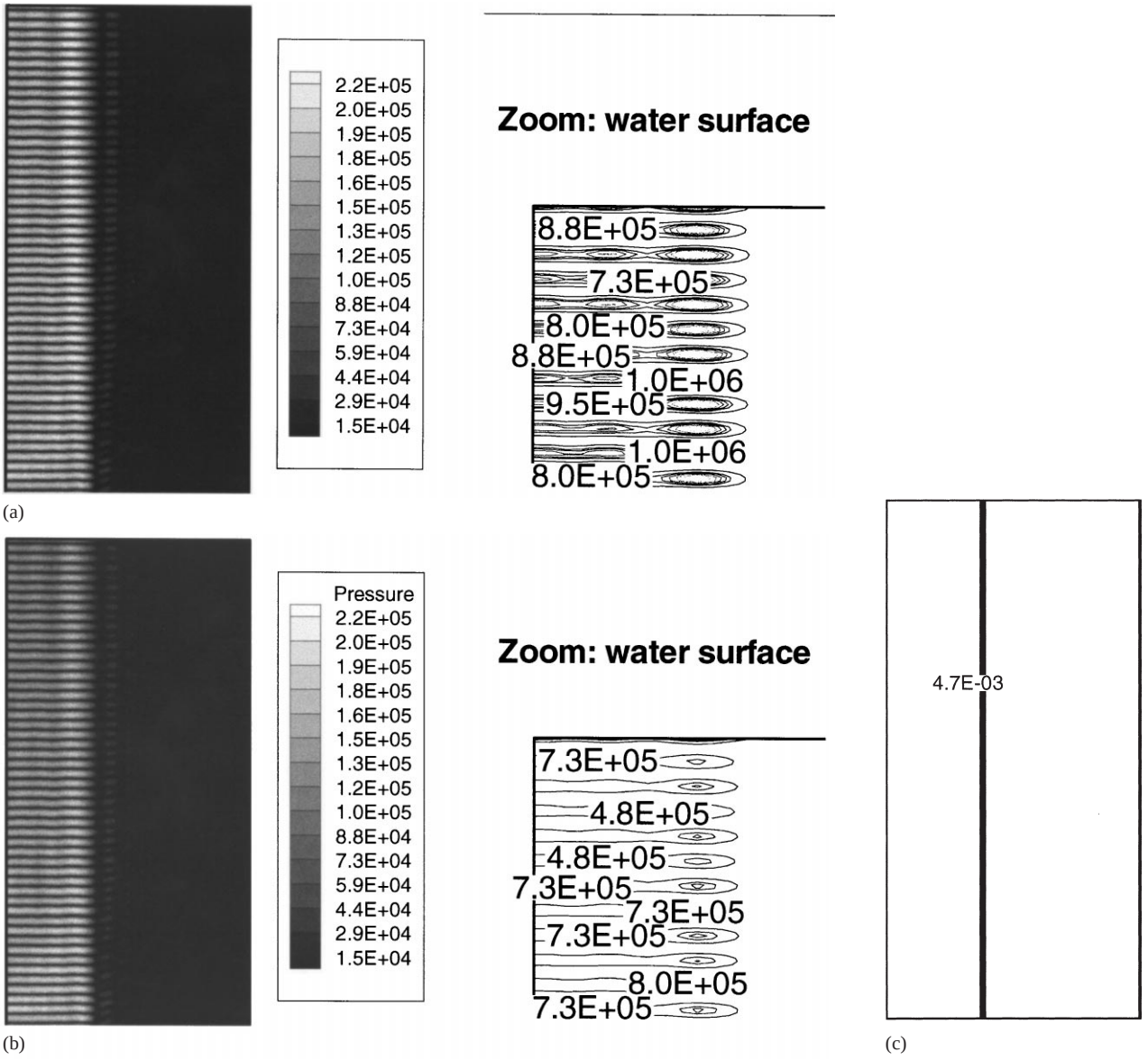

Fig. 2. Half-longitudinal view of the absolute pressure field distribution with no bubbles in the fluid (a), with the emergence of bubbles (b), at $t =$ 0.1 ms; 'A' bubble volume fraction due to the acoustic driving (c).

5.2. Bubble motion due to pressure gradient

The emerged 'A' bubbles collapse in the next cycle, and give birth to transient bubbles 'B'. Experiments [3] show that these bubbles move to pressure nodes. Because the damping is light, we assume a stationary non-streaming liquid. Thus we shall assume that pressure gradients are mainly responsible of the bubbles' migration. We assume that the daughter bubbles 'B' have the same equilibrium radius, set at 10 μm. The cartography of bubbles 'B' is that of the 'A' bubbles (Fig. 2(c)).

Fig. 3 shows the average bubble velocity intensity field. In the vicinity of the water surface, it is darker: because the wave is damped; the bubble velocity will be damped as well, since the bubble velocity is directly proportional to the pressure field (through the Bjerknes force).

Looking at the spatio-temporal evolution of bubbles clouds (Fig. 4), we see that 'B' bubbles tend to move to pressure nodes. This behaviour agrees with the theory [25]: bubbles with an equilibrium radius above the resonance size tend to migrate to the pressure nodes. When they reach the pressure nodes, experiments [3] show that 'B' bubbles disappear bumping into spider-like clouds. Their daughter bubbles ('C' bubbles) grow by rectified diffusion and levitate.

The' collapse of the 'B' bubbles and the pulsation of stable bubbles ('C' bubbles) at pressure nodes are responsible of the chemical activity of ultrasound [26,27]. Thus, Fig. 4(c) gives us a cartography of privileged sites of the chemical reactions.

5.3. Degassing of the fluid: hypothesis

Experiments show that some of the stable cavitation bubbles are torn off the pressure nodes. We assume that 10% of stable bubbles follow the fluid motion. We consider that the water–air interface is at equilibrium. Thus it is modelled as a free surface (velocity component perpendicular to the surface equals zero) for the fluid phase. Concerning the boundary conditions for the bubble phase, experiments show that no bubble evaporates in the 'cylindrical zone' defined by the wave propagation [3]. So the water–air interface is modelled as a free surface for this zone, and a free outlet for the complementary part of the interface, to take into account the bubble evaporation.

5.4. Results

The fluid main stream is around the axis of the sonoreactor, see Fig. 5(a). The value of the time-averaged fluid velocity is up to 1.6 cm s^{-1}. As expected, fluid motion is mainly induced by the temperature gradient occurring within the reactor (Figs. 5(a) and 6(b)). Computed velocity vectors are closed to experiments (Figs. 5(a) and 6(a)). Comparing fluid and bubble flow (Fig. 5(a) and (b)), we can deduce that bubble motion is mainly determined by the water flow. The maximal value of the time-averaged bubble velocity is 2.1 cm s^{-1}. Relative velocity values ($u_2 - u_1$) are positive (Fig. 5(c)). This is due to the buoyancy force that makes bubbles go up. This acceleration is counterbalanced by

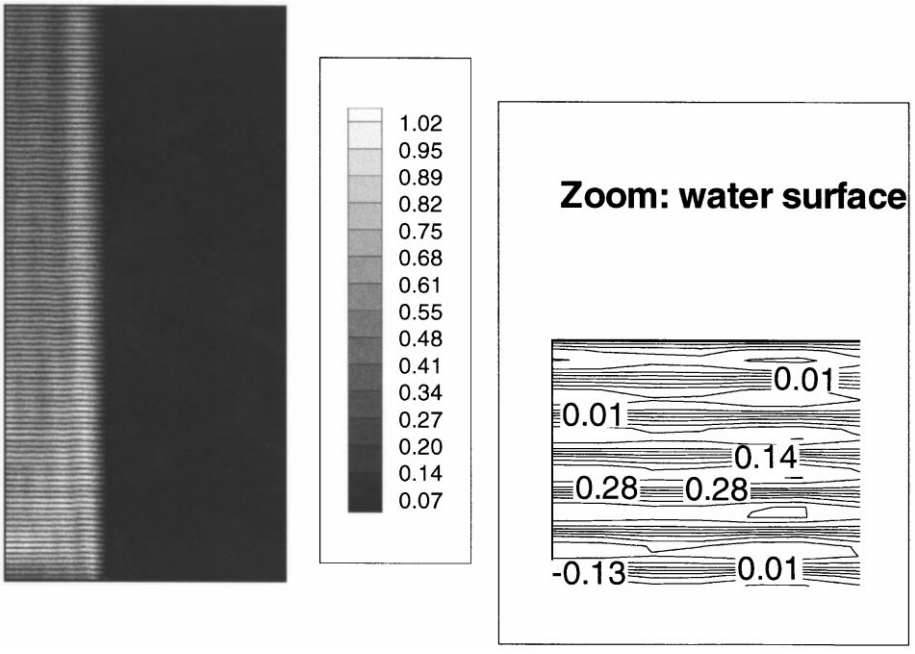

Fig. 3. Half-longitudinal view of the time-averaged 'B' bubble velocity intensity field due to the acoustic driving, in m s^{-1}.

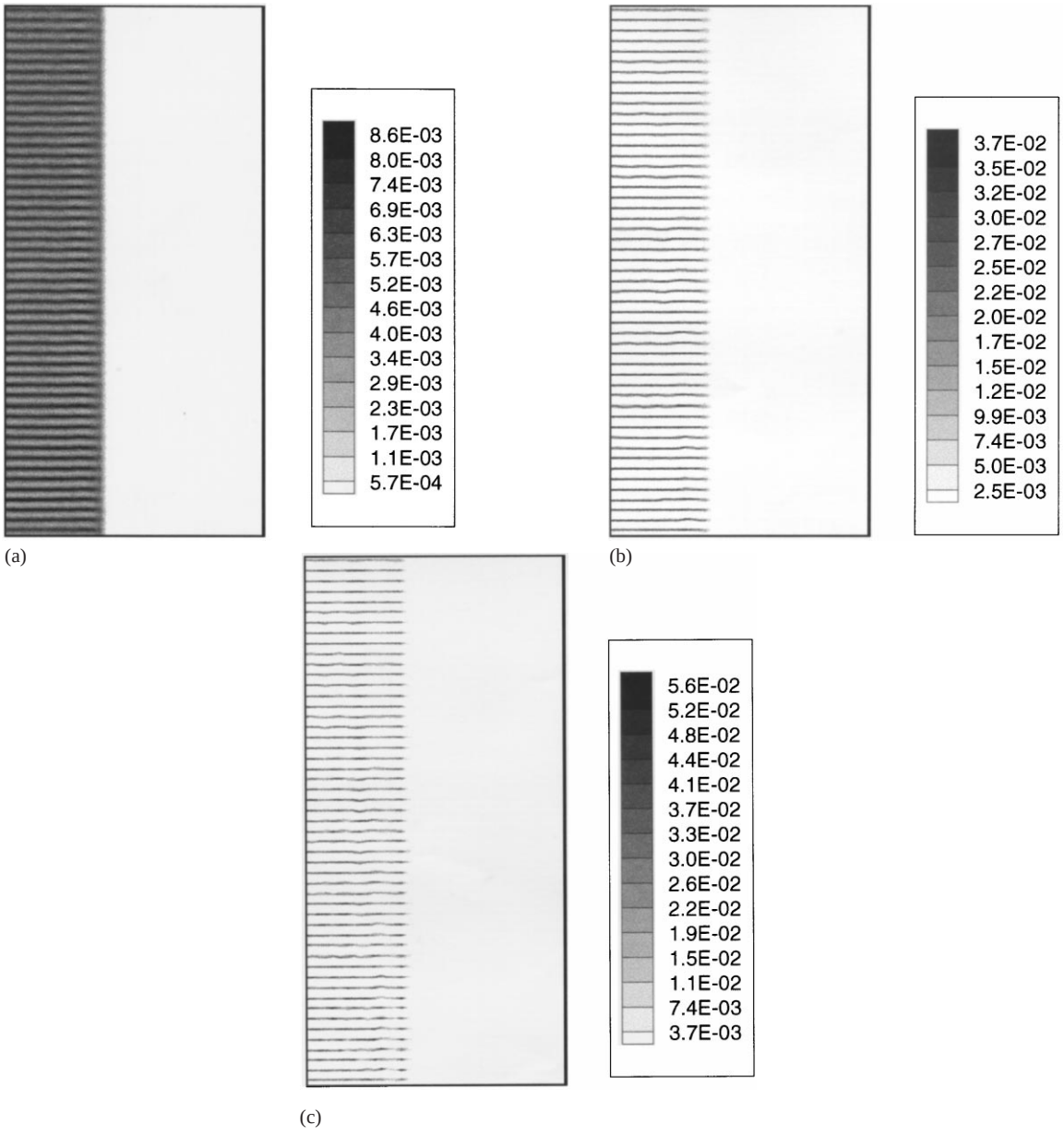

Fig. 4. Half-longitudinal view of 'B' bubble volume fraction at time $t=0.5$ ms (a), $t=3$ ms (b) and $t=10$ ms (c).

the drag and added mass forces. At equilibrium, the value of the resulting relative velocity is around 5 mm s^{-1}.

If we compare the bubble field at times $t=10$ ms and $t=1.2$ s (Figs. 4(c) and 7(a)), according to bubble velocity field we see that bubble displacement is greater in the vicinity of the reactor axis. At time $t=1.2$ s, bubbles accumulate under the water surface, owing to the ascendant movement and because they cannot evaporate, they follow the water–air interface. When they reach the 'wave propagation zone', some of them evaporate because of the buoyancy force. As for the others, their motion is induced by the fluid motion (Fig. 7(b)). Thus they move parallel to the free surface, and accumulate in a region where the horizontal component of the fluid velocity is zero. Then under the action of the buoyancy force, they evaporate. All the bubbles have evaporated at time 6 s.

6. Conclusion

It has been shown that to determine the spatio-temporal evolution of cavitation bubbles, we have to deal with different coupled phenomena. A continuum model taking into account interaction between bubbles, the sound field and the cavitation threshold permits us to determine the bubbles' emergence sites within the

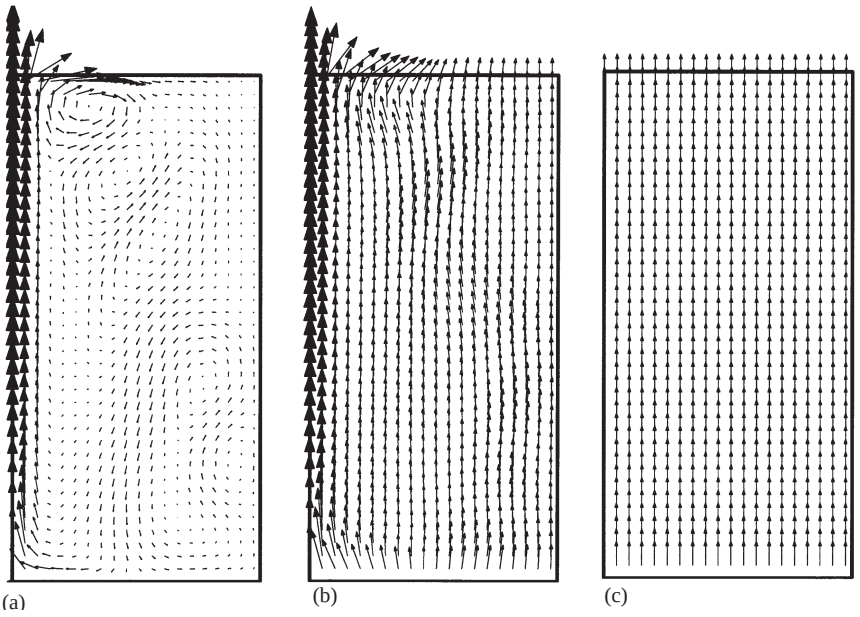

Fig. 5. Half-longitudinal view of time-averaged fluid velocity field (a), 'C' bubble velocity field (b), and relative velocity field (c) due to temperature gradient occurring in the fluid, in m s^{-1}.

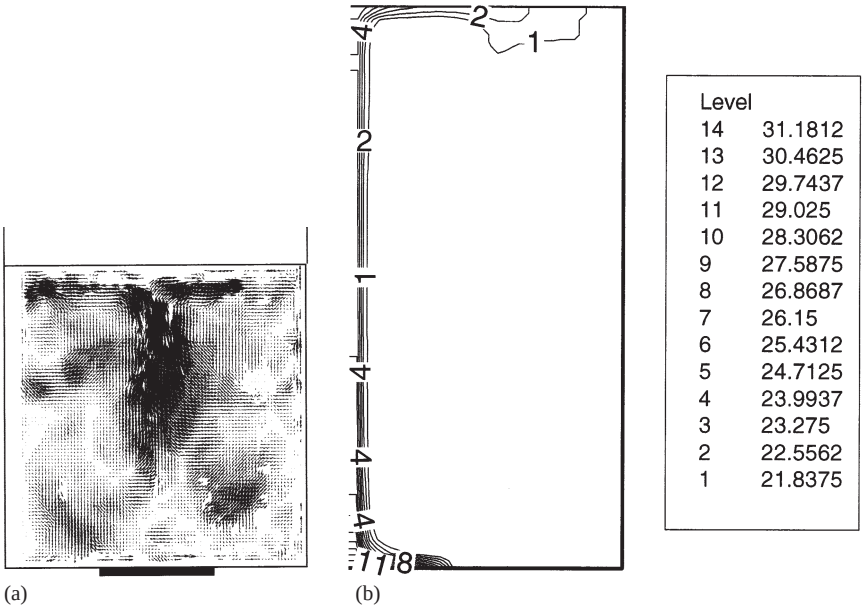

Fig. 6. Longitudinal view of velocity vectors measured by particle image velocity (a), and half-longitudinal view of the average temperature field (b).

reactor. The knowledge of the pressure field in the bubbly liquid allows us to determine forces applied on the bubbles. Calculation using an Eulerian two-fluid approach gives the spatio-temporal evolution of these bubbles. The main result is that bubbles tend to migrate at the pressure nodes. Knowing that these bubbles are responsible for the chemical activity of ultrasound, the computed cartography of bubbles' accumulation sites give insight into the chemical cartography within the reactor. Computation of the fluid motion due to temperature gradients occurring within the fluid (because of the heating transducer) with interaction with the bubbles taken into account explain degassing of the fluid. Bubbles tend to move to the water surface, and the action of the buoyancy force makes them evaporate by reaching the water–air interface.

Future improvements of the models should include, for instance, a more sophisticated law on the bubble emergence, such as a linear variation of the bubble volume fraction with the pressure amplitude. Concerning the spatio-temporal evolution of the bubble clouds, streaming of the liquid due to non-linear effects should

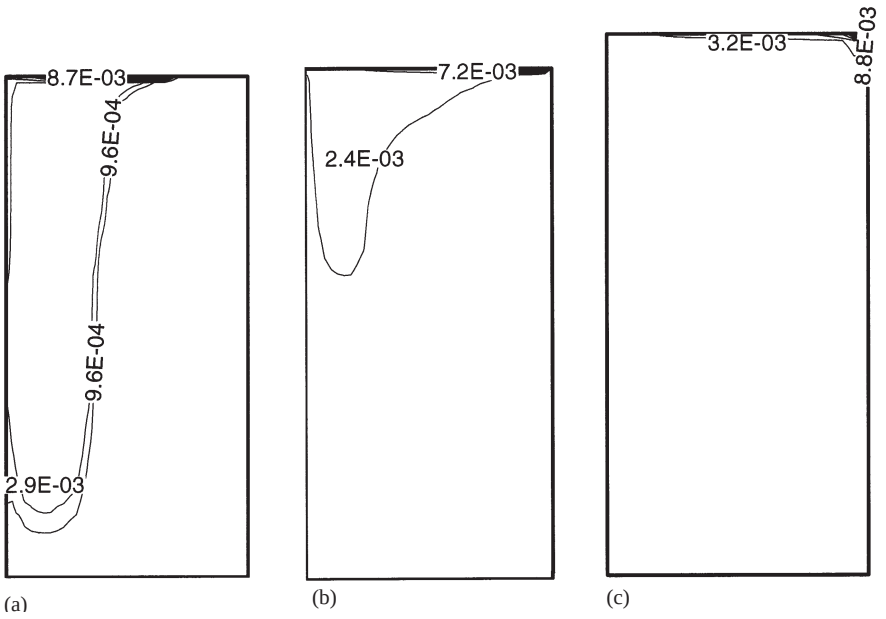

Fig. 7. Half-longitudinal view of 'C' bubble volume fraction at time $t=1.2$ s (a), $t=2.2$ s (b), and $t=3$ s (c).

be included in the model, as well as the secondary Bjerknes forces that act between bubbles. Concerning the degassing of the fluid, evaporation model has to be improved to take into account surface tension effects occurring at the free surface.

Acknowledgements

The authors are grateful to Electricité de France for financial support and wish to thank F. Gélix, O. Simonin and S. Vincent for constructive discussions.

References

[1] F.R. Young, Cavitation, McGraw-Hill, London, 1989.
[2] L.A. Crum, A.I. Eller, Motion of bubbles in a stationary sound field, J. Acous. Soc. Am. 48 (1970) 181.
[3] J.L. Laborde, Modélisation d'un fluide soumis à des ultrasons de puissance, Ph.D. Thesis, Univ. Bordeaux I, 1998.
[4] C. Horst, Y.S. Chen, U. Kunz, U. Hoffmann, Design, modeling of a novel sonochemical reactor for heterogeneous reactions, Chem. Eng. Sci. 51 (1996) 1837–1846.
[5] S. Dähnke, K.M. y, F.J. Keil, Modeling of three-dimensional pressure fields in sonochemical reactors with an inhomogeneous density distribution of cavitation bubbles. Comparison of theoretical and experimental results, Ultrason. Sonochem. 6 (1999) 31–41.
[6] S. Dähnke, F.J. Keil, Modeling of three-dimensional linear pressure fields in sonochemical reactors with homogeneous and inhomogeneous density distribution of cavitation bubbles, Ind. Eng. Chem. Res. 37 (1998) 848–864.
[7] S. Dähnke, K.M. y, F.J. Keil, A comparative study on the modeling of sound pressure field distributions in a sonoreactor with experimental investigation, Ultrason. Sonochem. 6 (1999) 221–226.
[8] Sochard, Modélisation de la cavitation acoustique et de l'activation de réactions homogènes, thèse de doctorat, école ENSIGCT.
[9] O. Louisnard, Contribution a l'étude de la propagation des ultrasons en milieu cavitant, thèse d'état, Ecole des Mines de Paris, 1998.
[10] R.E. Caflisch, M.J. Miksis, G.C. Papanicolaou, L. Ting, Effective equations for wave propagation in bubbly liquids, J. Fluid Mech. 153 (1985) 259–273.
[11] K.W. Commander, A. Prosperetti, Linear pressure waves in bubbly liquids: Comparison between theory and experiments, J. Acous. Soc. Am. 85 (1989) 732–746.
[12] F. Burdin, P. Guiraud, A.M. Wilhelm, H. Delmas, Investigatin of the acoustic cavitation field by the phase Doppler technique: influence of acoustic and physico-chemical parameters, Proceedings 2nd Conference: Applications of Power Ultrasound in Physical and Chemical Processing, Toulouse, 6–7 May, (1999).
[13] F.G. Blake, Tech. Memo. no. 9, Acoustics Research Laboratory, Harvard University, MA, 1949.
[14] L. Van Wijngaarden, On the equations of motion for mixtures of liquid and gas bubbles, J. Fluid Mech. 33 (3) (1968) 465–474.
[15] J.B. Keller, I.I. Kolodner, Damping of underwater explosion bubble oscillations, J. Appl. Phys. 27 (1956) 464–467.
[16] A. Properetti, Thermal effects and damping mechanisms for the forced radial oscillation of gas bubbles in liquids, J. Acoust. Soc. Am. 65 (1977) 17.
[17] J.F. Figué, Modélisation numérique des écoulements compressibles en milieu poreux. Application à la détente de Joule–Thomson, Ph.D. Thesis, Univ. Bordeaux I, 1996.
[18] D. Thai Van, J.P. Minier, O. Simonin, P. Freydier, P. Olive, Multidimensional two-fluid model computation of turbulent two-phase flows, Proc. Int. Symp. on Numerical Methods for Multiphase Flows, ASME FED 185 (1994) 227–291.
[19] R. Bel Fdhila, O. Simonin, Eulerian prediction of a turbulent bubbly flow downstream of a sudden pipe expansion, Erlangen, M. Sommerfeld, Bilateral Seminars of the International Bureau/Forschungszentrum Jülich GmbH 14 (1993) 264–273.
[20] A. Eller, Force on a bubble in a standing acoustic wave, J. Acoust. Soc. Am. 43 (1968) 170.
[21] R. Mettin, S. Luther, C.D. Ohl, W. Lautherborn, Acoustic cavita-

tion structures and simulations by a particle model, Ultrason. Sonochem. 6 (1999) 25.
[22] J. Magnaudet, D. Legendre, The viscous drag force on a spherical bubble with a time-dependent radius, Phys. Fluid 10 (1997) 550–554.
[23] N. Gondrexon, V. Renaudin, P. Boldo, Y. Gonthier, A. Bernis, C. Petrier, Degassing effect and gas–liquid transfer in a high frequency sonochemical reactor, Chem. Eng. J. 66 (1997) 21–26.
[24] R. Clift, J.R. Grace, M.E. Weber, Bubbles, Drops, and Particles, Academic Press, New York, 1978.
[25] T.G. Leighton, The Acoustic Bubble, Academic Press, London, 1994.
[26] A. Henglein, Sonochemistry: historical developments and modern aspects, Ultrasonics 25 (1989) 6–16.
[27] K.S. Suslick, D.A. Hammerton, R.E. Cline, The sonochemical hot spot, J. Am. Chem. Soc. 108 (1986) 55 641–55 643.